

Structure and Magnetism of EuS on Bi₂Se₃(0001)

Holger L. Meyerheim,* Arthur Ernst, Katayoon Mohseni, Andrey Polyakov, Igor V. Maznichenko, Pawel A. Buczek, Alessandro Coati, and Stuart S. P. Parkin

The rocksalt-type ferromagnetic (FM) insulator EuS (bulk $T_C = 17$ K) grown on Bi₂Se₃ with well-matched (111) plane of the film and (0001) plane of the substrate is studied. The system may feature magnetic proximity effect breaking the time-reversal symmetry and opening a bandgap in the metallic topologically protected surface state of Bi₂Se₃. The experimental X-ray diffraction studies are combined with ab initio calculations to resolve contradictory results concerning the enhancement of the T_C up to 300 K and the degree of induced magnetization in the system. It is concluded that previous studies relied on idealized and unconfirmed structure models. Herein, it is shown by surface X-ray diffraction (SXRD) with ab initio calculations that a two double layer-thick EuS film grows with a sharp interface and without chemical intermixing in a single domain state in an FCC-type stacking on the Bi₂Se₃(0001) surface in which the topmost layer is metallic, thereby lifting polarity. A large p_z -orbital-derived top-layer sulfur magnetic moment of 0.6 μ_B is found, whereas for europium, $\mu_{Eu} = 6.9 \mu_B$ throughout the film is found. No magnetization within the first Bi₂Se₃ quintuple layer is found. The calculation of the exchange parameters J_{ij} indicates a complex FM and antiferromagnetic ordering between europium and sulfur with a maximum Néel temperature of 226 K.

the most prominent phase due to its large bulk bandgap of the order of 0.3 eV. Topological protection can be lifted by a magnetic field oriented perpendicular to the surface involving an opening of a gap at the Dirac point (D_P). The latter is of utmost importance in the context of potential novel spintronic device applications which involve dissipation less transport of spin-polarized charge carriers exploiting the quantum anomalous hall effect (QAHE).^[1–5]

To establish ferromagnetic (FM) ordering in TIs, several proposals have been made. For instance, one approach is doping of “bulk” TIs with magnetic species like iron, vanadium, chromium, and manganese.^[2,5,6–19] It is generally argued that bulk dopants replace bismuth in the crystal structure, i.e., they occupy substitutional sites.^[9,12,13,15,18,20,21] The disadvantage of the bulk doping approach is that the dopant’s concentration is limited to ≈ 5 –10% only, as at higher concentrations the precipitation of the dopant sets in and

the structural integrity of the TI is not preserved in general.


In our research conducted in the context of the “Schwerpunktprogramm” (Priority Programme) SPP1666 (“Topological Insulators: Materials—Fundamental Properties—Devices”) funded by the Deutsche Forschungsgemeinschaft (DFG), we have followed a different approach to overcome the bulk doping concentration limitation by surface doping. In the ultrathin film limit, new phases can be prepared which are metastable and in which dopants might be incorporated in

1. Introduction

During the past decade, the study of topological insulators (TIs) has become a major branch in solid-state physics. TIs are insulators in the bulk, whereas their surface is metallic related to a spin-polarized surface state. Importantly, this surface state is topologically protected by time reversal symmetry. Examples for TIs are the chalcogenides of bismuth and antimony, such as Bi₂Se₃, Bi₂Te₃, and Bi₂S₃. Among them, Bi₂Se₃(0001) is

Dr. H. L. Meyerheim, Prof. A. Ernst, Dr. K. Mohseni, Dr. A. Polyakov, Prof. S. S. P. Parkin
Max-Planck-Institut für Mikrostrukturphysik Halle
Weinberg 2, Halle 06120, Germany
E-mail: holger.meyerheim@mpi-halle.mpg.de

Prof. A. Ernst
Institut für Theoretische Physik
Johannes Kepler Universität
Linz 4040, Austria

 The ORCID identification number(s) for the author(s) of this article can be found under <https://doi.org/10.1002/pssb.202000290>.

© 2020 The Authors. Published by Wiley-VCH GmbH. This is an open access article under the terms of the Creative Commons Attribution License, which permits use, distribution and reproduction in any medium, provided the original work is properly cited.

DOI: 10.1002/pssb.202000290

Dr. I. V. Maznichenko
Institut für Physik
Martin Luther Universität Halle-Wittenberg
Halle 06099, Germany

Dr. I. V. Maznichenko, Prof. P. A. Buczek
Department of Engineering and Computer Sciences
Hamburg University of Applied Sciences
Berliner Tor 7, Hamburg 20099, Germany

Dr. A. Coati
Synchrotron SOLEIL
L’Orme des Merisiers Saint-Aubin
BP 48, Gif-sur-Yvette Cedex 91192, France

concentrations largely exceeding bulk limits.^[22–26] This approach, by which the magnetic proximity is exploited to establish FM order in the TI has been shown to be very successful in the case of Fe deposited on $x = 9\%$ Mn-doped $\text{Bi}_{(1-x)}\text{Mn}_x\text{Te}$,^[27] where T_C was reported to be as high as room temperature. However, as shown by several investigations, we have published in the recent past during the course of this project, direct surface deposition of metals in general involves an uncontrolled reaction at the interface which modifies the near surface geometric and electronic structure.^[24,25,28–30] In consequence, for the controlled preparation of a structurally homogeneous and sharp interface, deposition of an (anti) FM or FM insulator film is a promising route.

In this respect, the FM insulator EuS is a primary candidate to serve as an adsorbate. Bulk EuS is a ferromagnet with $T_C = 17$ K and its crystal structure (cubic rocksalt type with lattice parameter $a_0 = 5.968$ Å at 298.15 K) fits well for an almost lattice matched growth with its (111) plane parallel to the (0001) surface of Bi_2Se_3 (4.22 vs 4.14 Å, respectively). Consequently, the epitaxial system EuS/ Bi_2Se_3 (0001) has already been investigated in the past.

Proximity-induced ferromagnetism with T_C in the 20 K range has been reported for EuS deposited on undoped Bi_2Se_3 ^[31] using magnetotransport measurements. An excess magnetic moment as compared with that which can be expected from the magnetic moment of Eu^{2+} ions alone (11.3 vs $7\mu_B$ per Eu^{2+} ion) was observed. This was attributed to the induced magnetization in Bi_2Se_3 , either by magnetization of the bismuth atoms or of the electron gas of the topological surface state (TSS). Subsequently, a theoretical study by Ereemeev et al.^[32] challenged the interpretations of the study by Wei et al.^[31] The calculations were based on the structure model in which the interfacial Eu^{2+} ions are located in the face-centered cubic (FCC)-type site of the Se-terminated Bi_2Se_3 (0001) surface. As pointed out in the study by Ereemeev et al.,^[32] the very localized 4f electronic states of the rare-earth ion Eu^{2+} are not capable to provide an efficient proximity effect and the induced magnetic moment within the TI is negligibly small. The only interaction between EuS and Bi_2Se_3 originates from the overlap between the TSS with the topologically trivial metallic interface states. The latter originate from EuS adsorption-induced band bending. An alternative interpretation for the results in the study by Wei et al.^[31] was given by assuming some diffusion of europium across the interface replacing bismuth and/or selenium.

More recently, experimental works^[33,34] have reported the enhancement of the magnetization within the top Bi_2Se_3 quintuple layer (QL), enhancement of T_C of the EuS film to $T_C \approx 300$ K and a very strong out of plane magnetic anisotropy,^[33] the latter being a prerequisite for breaking time reversal symmetry. It has been suggested that in addition to the strong spin orbit coupling in Bi_2Se_3 , it is the penetration of the TSS into the EuS film, which is responsible for the T_C enhancement in EuS resulting from Ruderman–Kittel–Kasuya–Yosida (RKKY)-type exchange interaction.

Despite intense discussion regarding the proximity-induced magnetization in the epitaxial EuS/ Bi_2Se_3 system, theory up to now relies on the interface structure model in which europium atoms of the first EuS (double) layer are located in the FCC-type threefold hollow sites formed by the topmost selenium atoms, i.e., they are located above the third-layer selenium atoms.

Further layers are stacked such as to continue the FCC-stacking. Until now, it is not clear whether this model is correct. Transmission electron microscopy images^[33] indicated very good epitaxial growth but a detailed atomic structure could not be derived. As already noted in the study by Wei et al.,^[31] a clear-cut understanding of the proximity-induced interface magnetism would require the in-depth analysis of the interface structure. To this end, we have carried out a synchrotron radiation X-ray diffraction study of the EuS/ Bi_2Se_3 (0001) interface.

2. Growth Characterization of EuS/ Bi_2Se_3 (0001)

Prior to the surface X-ray diffraction (SXRD) experiments growth of EuS on Bi_2Se_3 (0001) was characterized by low-energy-electron diffraction (LEED) and scanning tunneling microscopy (STM). The experiments were conducted in an ultrahigh vacuum (UHV) chamber equipped with standard surface characterization tools. The (0001) surface of the bulk Bi_2Se_3 single crystal was cleaned by repeated Ar^+ -ion sputtering ($E_{\text{kin}} = 1$ keV) followed by annealing at about 480 °C for about 30 min. Surface cleanliness and surface morphology were characterized by Auger electron spectroscopy (AES) and STM.

The LEED pattern shown in **Figure 1a** recorded at an electron energy of $E = 30$ eV is typical for the well ordered and smooth Bi_2Se_3 (0001) surface prepared by this procedure.^[22,23] We have selected an electron energy so as to maximize the contrast between symmetry in-equivalent first-order reflections. According to the threefold symmetry of the Bi_2Se_3 (0001) surface (plane group $p3m1$), two sets of reflections are observed, the stronger set being highlighted by the circles, the weaker one by the arrows.

EuS deposition was subsequently carried out in situ by evaporation of 3 N EuS powder from a well-degassed Knudsen cell heated up to 870 °C. At this temperature, growth of one EuS double layer (DL) requires a deposition time of about 1 h. Here and in the following, we define as one DL one single sheet consisting of one europium and one sulfur layer, which is the building block of the cubic rocksalt EuS structure along

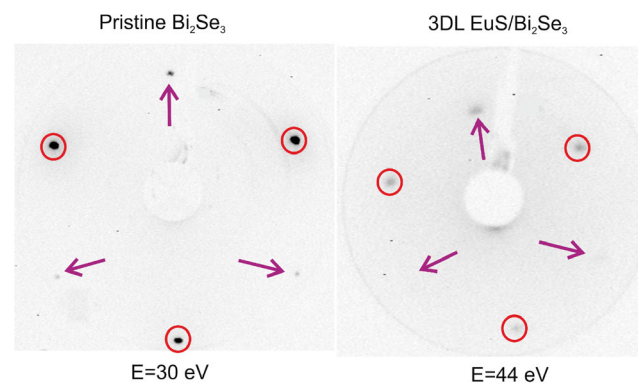


Figure 1. LEED patterns shown in an inverse contrast of a) pristine and b) EuS covered Bi_2Se_3 (0001) surface. Electron energies in electron volts are listed below the panels. EuS deposition leaves the threefold symmetric (1×1) surface lattice metric unchanged indicating the formation of a well-ordered EuS overlayer lattice matched to the substrate. The two sets of symmetry-related spots are highlighted by circles and arrows, respectively. The uppermost spot appears stronger than the two equivalent one due to some tilting of the crystal. For details see text.

the bulk [111] direction. During deposition, the pressure remained in the 10^{-9} mbar range. After deposition, the sample was annealed at 460 °C for about 15 min to improve the long-range order of the film. Chemical characterization was carried out by AES, which showed that the differentiated S-KLL transition peak-to-peak amplitude at $E = 152$ eV is about as intense as those of the Bi–NOO transitions ($E = 96$ and 101 eV). AES spectra of Bi_2Se_3 are discussed in detail in the study by Roy et al.^[23] Due to the low sensitivity of the $\text{Eu-N}_{45}\text{O}_{23}\text{N}_{67}$ and the $\text{N}_{45}\text{O}_{67}\text{N}_{67}$ AES transition near 109 and 120 eV^[35] and their overlap with Bi–NOO peaks, they could not be determined unambiguously. Nevertheless, X-ray photoemission spectroscopy (XPS) using a Mg $K\alpha$ X-ray source showed the presence of europium in the deposited film.

A LEED pattern of an approximately three DL-thick EuS film is shown in Figure 1b recorded at $E = 44$ eV. As compared with those observed for the pristine surface, the spots are not notably

broadened, only the signal-to-background ratio has become smaller. As in the case of the pristine sample, the LEED pattern exhibits a threefold symmetry. The observation of the threefold symmetry for such a thick EuS film, where scattering by the substrate is negligible, is an important result. It proves that the EuS film adsorbs in a preferential way on the threefold symmetric $\text{Bi}_2\text{Se}_3(0001)$ surface rather than forming two mutually 60°-rotated domains which would result in a sixfold symmetric LEED pattern.

The surface morphology was investigated by STM. **Figure 2a** shows a $800 \times 800 \text{ nm}^2$ STM image ($U = 1 \text{ V}$, $I = 200 \text{ pA}$) of the three DL-thick EuS film (the same sample as used for the LEED experiments). The profile along the white line is plotted in Figure 2b. The morphology of the film surface is characterized by laterally 10–30 nm-sized islands homogeneously covering the 500 nm wide terraces of the substrate surface, whose step morphology remains unaltered upon EuS deposition. Steps on

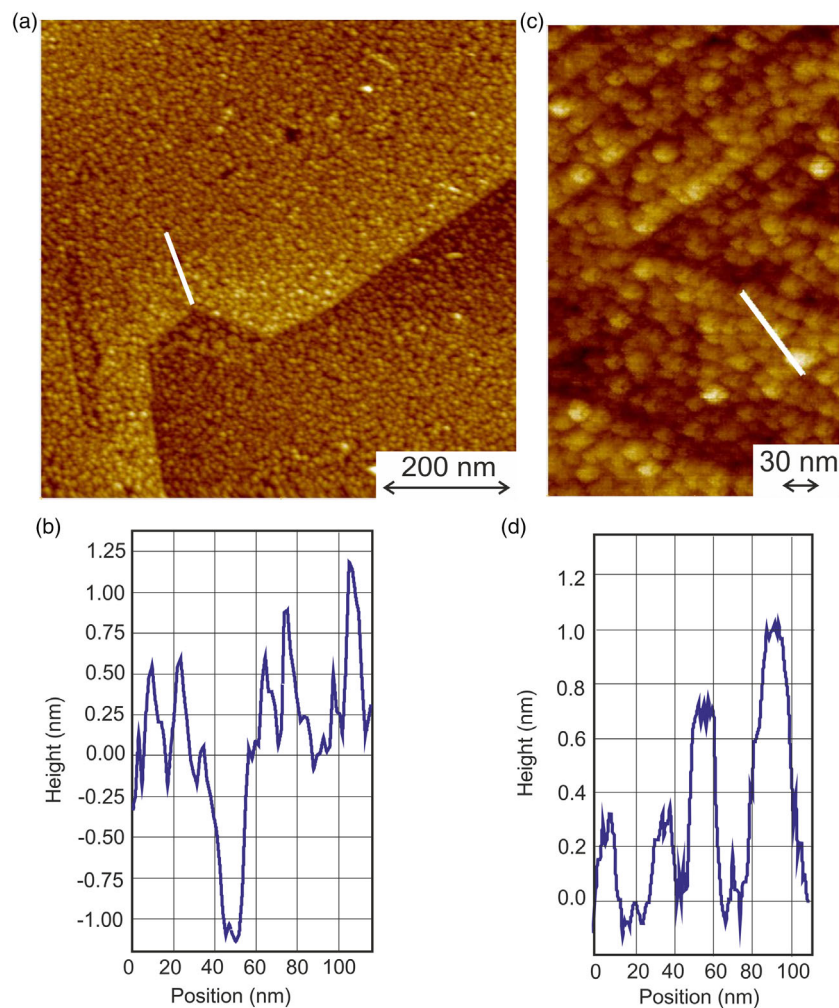


Figure 2. a) $800 \times 800 \text{ nm}^2$ constant current STM image ($U = +1.0 \text{ V}$, $I = 200 \text{ pA}$) of an approximately three DL-thick EuS film on $\text{Bi}_2\text{Se}_3(0001)$. The adsorbate layer is characterized by about 10–30 nm-sized islands homogeneously covering the terraces of the $\text{Bi}_2\text{Se}_3(0001)$ surface. The profile along the white line in (a) is shown in (b). Islands are about 1 nm high corresponding to three EuS DLs which at this coverage fill the majority of the surface. Some fraction of single-layer and DL EuS islands grow on the complete film. c) $300 \times 480 \text{ nm}^2$ STM image of the sample recorded in the vicinity of step edges. Islands align along the upper step edges more uniformly than on terraces. The line profile d) highlights different islands differing in height by 0.35 nm, i.e., one DL which is the building block during growth.

the $\text{Bi}_2\text{Se}_3(0001)$ surface are 0.96 nm high corresponding to the thickness of one QL, the basic building block of the Bi_2Se_3 bulk crystal.^[22,23] The vacancy island which the linescan crosses is about 1 nm deep, very closely corresponding to the thickness of three DLs along the [111] direction bulk EuS ($\sqrt{3} \times 0.5968 = 1.034$ nm). In addition, some islands grown on this layer have a height of about 0.6 and 1.0 nm, corresponding to two and three DLs, respectively. These observations suggest that growth of EuS takes place in units of one DL, about 0.35 nm thick.

This model is supported by the zoom-in image ($300 \times 480 \text{ nm}^2$) with the same tunneling parameters and a profile along the line is shown in Figure 2c,d, respectively. The islands fully cover the surface leaving the morphology of the surface (e.g., the V-shaped morphology of the step edges) unchanged. Closer inspection suggests that the islands located directly along the step edges are well aligned in some contrast to those on the terraces. The profile along the line confirms the conclusions that the growth of the film occurs in Eu–S DL. Islands along the line have a height which are multiples of 0.35 nm.

3. Structure of EuS/ $\text{Bi}_2\text{Se}_3(0001)$

SXRD experiments were conducted at the beamline SIXS of the Synchrotron Soleil in St. Aubin (France) using an UHV diffractometer equipped with a preparation chamber. The EuS/ $\text{Bi}_2\text{Se}_3(0001)$ sample was prepared in the same way as done in the home laboratory. Prior to the SXRD experiments, surface chemistry and long-range order were investigated by AES and LEED, yielding the same results as discussed earlier. As no superstructure is formed upon deposition of the EuS film, the SXRD structure determination is based on the analysis of the intensity distribution along the (1×1) integer-order crystal truncation rods (CTRs) in the same way as done for the majority of surface/interface systems studied during the SPP1666 project. In the following, the basics of the CTR SXRD analysis are shortly outlined:

3.1. SXRD and CTRs

To outline the basic principle of the structure analysis in Figure 3a, a schematic of the reciprocal space in an a^*-c^* section is shown together with the corresponding crystal model in (b) which is “semi-infinite” along the c -axis. As a consequence of the crystal termination, in addition to the bulk Bragg points (spheres), there exist rods normal to the sample surface which are represented by thin solid lines. These rods are referred to as “CTRs.” They were already theoretically predicted by v.Laue,^[37] but the first clear-cut experimental verification took until 1986 published by Robinson.^[38] The analytic treatment shows that in the case of a bulk truncated crystal the intensity along the CTRs varies by roughly five orders of magnitude between the in-phase bulk Bragg positions at integer ℓ and the antiphase condition half way between the bulk Bragg reflections. Consequently, at the antiphase condition, where the reflected intensity of a semi-infinite FCC-type crystal is calculated to be equal to that of a quarter of a monolayer, adsorption of foreign species commensurate with the substrate lattice substantially modifies the total reflected intensity.

The structure factor amplitude of a primitive crystal can be written as a semi-infinite sum over the lattice planes from $-\infty$ to zero

$$F_{\text{CTR}} = \sum_{n=-\infty}^0 f_s \cdot \exp[2i\pi\ell n] \cdot g(h) \cdot g(k) \quad (1)$$

$$= \frac{f_s}{1 - \exp[-i2\pi\ell]} \cdot g(h) \cdot g(k) \quad (2)$$

with f_s being the atomic scattering amplitude of the substrate atoms. The finite penetration of the X-ray beam was neglected. The latter, expressed by an effective absorption factor $\exp[-\mu \cdot n \cdot d]$ (with d being the layer spacing and μ the absorption coefficient) lifts the divergence of the lattice sum at the bulk Bragg conditions at integer ℓ . We have explicitly considered

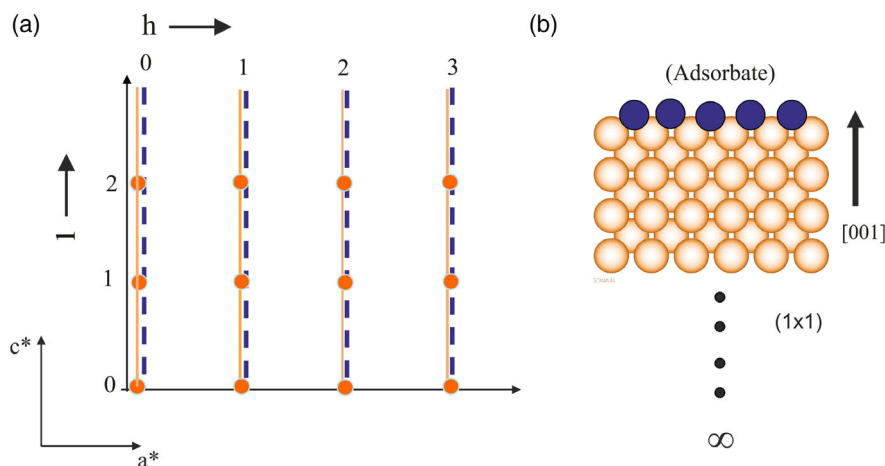


Figure 3. a) Schematic of the reciprocal space in an a^*-c^* section. The corresponding crystal structure is shown in (b). Bulk Bragg reflections of the semi-infinite crystal are represented as spheres at integer positions h and ℓ . The truncation of the crystal gives rise to rods along c^* (solid line). Adsorption of an adlayer atoms commensurate with the substrate involves a coherent addition of the scattering amplitudes between the rods of the substrate and those of the adsorbate, the latter represented by the dotted lines. Reproduced with permission.^[36] Copyright 2019, Wiley-VCH.

only the summation along the z -direction (surface normal) and included the contributions along the a and b directions in the "Laue factors" $g(h)$ and $g(k)$.^[37] Adsorption of any species as well as relaxations of the substrate being commensurate with the substrate lattice can be simulated by coherent addition of F_{CTR} with the adsorbate amplitude to give the total scattering amplitude (F_{tot}) which can be expressed by

$$F_{\text{tot}} = F_{\text{CTR}} + \sum_j f_{\text{ad}} \cdot \theta_j \cdot \exp[i2\pi(hx_j + ky_j + \ell z_j)] \quad (3)$$

with the atomic scattering factor f_{ad} of the adsorbate and its fractional coverage θ_j . The summation runs over all atoms j within the (1×1) surface unit cell.

3.2. Atomic Structure of EuS/Bi₂Se₃(0001)

For the data collection, we used a wavelength of $\lambda = 0.103$ nm ($E = 12.0$ keV) of the beam incident at an angle of $\alpha_i = 0.5^\circ$ to the sample surface. Integrated intensities (I_{obs}) were recorded using a 2D pixel detector in two different ways by successive conventional transverse (ω -) scans at a given q_z and by direct line scans along q_z , the momentum transfer along the reciprocal c^* direction normal to the surface. Both data sets give the same results. The I_{obs} were derived from the raw data and converted to structure factor magnitudes ($|F_{\text{obs}}|$) using the program "Binoculars" as outlined in the study by Drnec et al.^[39] In the following, we refer to the data derived from transverse ω -scans.

Figure 4 shows the intensity distribution along five symmetry independent CTRs which were obtained by symmetry averaging from in total ten CTRs. Symbols represent the $|F_{\text{obs}}|$ together with their (1σ) standard deviations derived from the quadrature sum of the statistical and the systematic error as outlined, e.g., in the study by Robinson and Tweet.^[40] We find the reproducibility

of symmetry equivalent $|F_{\text{obs}}(\text{HKL})|$ being equal to about 10%. The data set consists of in total 951 data points separated by 0.05 reciprocal lattice units (rlu) along q_z with a maximum q_z of 15.45 rlu along the (20L) rod. We refer to the lattice of the Bi₂Se₃ crystal with $a_0 = b_0 = 4.14$ Å, and $c_0 = 28.65$ Å, respectively.

The $|F_{\text{obs}}|$ were fitted using the Program "Prometheus" adapted to include the CTR analysis.^[41] Due to the high symmetry of the structure (plane group $p3m1$) in which all atoms occupy high-symmetry sites (Wyckoff sites 1a, 1b, and 1c), only the z -parameters of the atomic sites are free parameters in addition to an overall scale factor and the Debye parameter ($B = 8\pi U$, with U being the isotropic mean square displacement amplitude) representing static and dynamic disorders.^[42] The structure of the pristine Bi₂Se₃(0001) surface has been thoroughly investigated in our group in the past.^[22,23] Comparison of the data in Figure 4 with those published in the studies by Roy et al.^[22,23] evidences that the overall shape of the CTRs is strongly modified upon EuS adsorption.

The best fit of the $|F_{\text{calc}}(\text{HKL})|$ to the $|F_{\text{obs}}(\text{HKL})|$ is represented by the solid line in Figure 4. The fit quality is quantified by the unweighted residuum (R_U) ($R_U = \sum ||F_{\text{obs}}| - |F_{\text{calc}}|| / \sum |F_{\text{obs}}|$. Here, F_{obs} and F_{calc} are the experimental and calculated structure factors, respectively. The summation runs over all data points.) and by the Goodness of Fit (GOF) parameter ($\text{GOF} = \sqrt{1/(N - P) \cdot \sum [(I_{\text{obs}} - I_{\text{calc}})^2 / \sigma^2]}$, with: $I = |F|^2$, σ = standard deviations of the data points, N = number of data points, P = number of parameters.) for which $R_U = 0.17$ and $\text{GOF} = 1.21$ is obtained, respectively. These values can be considered as fairly good and direct-eye inspection of Figure 4 also indicates that the fit follows the data in detail.

The structure model derived from the fit is schematically shown in Figure 5. We have considered the first QL of the Bi₂Se₃ substrate only, all deeper layers were treated as bulk like.

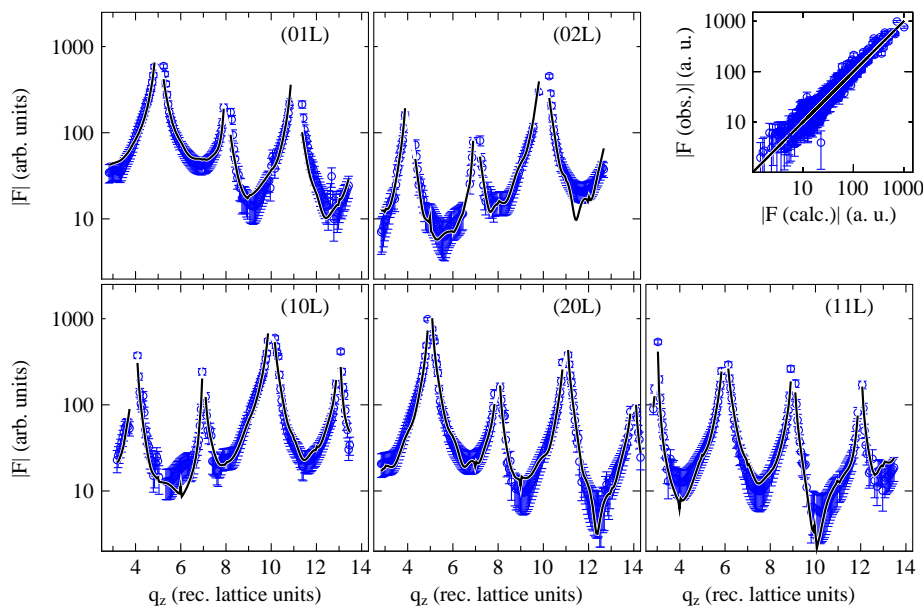


Figure 4. Experimental (symbols) and calculated (lines) structure factor magnitudes ($|F_{\text{obs}}|$, $|F_{\text{calc}}|$) along five symmetry independent CTRs. The fit corresponds to the structure model discussed using Figure 5.

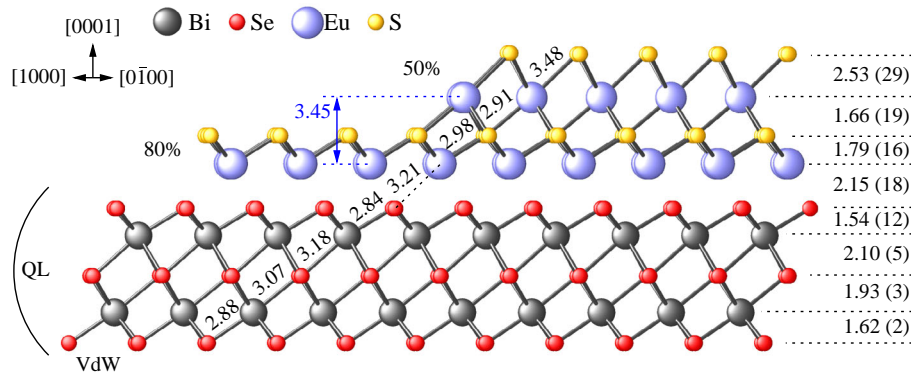


Figure 5. Structure model of the EuS/Bi₂Se₃(0001) interface. Differently colored spheres represent sulfur, europium, bismuth, and selenium atoms as labelled in the legend. Interlayer and interatomic distances are given in Ångströms. The fractional occupancy of each layer is approximately represented by number of spheres.

Atoms are represented by differently colored spheres as shown in the legend. Numbers refer to interatomic and interlayer distances in Ångströms. The most important result is that EuS grows with first-layer europium atoms located in the threefold hollow (“FCC”) site above the third-layer selenium atom. The following selenium layer also continues the FCC-type stacking.

We have analyzed the structure in very detail by setting different occupancy factors (θ) for the different layers while simultaneously relaxing the z -coordinates and the atomic displacement parameters (ADPs), here given by the Debye parameter (B).^[42] **Figure 6** shows a contour plot of the GOF parameter versus the fractional occupancy of the first DL growing by FCC and/or hexagonal close packed (HCP)-type stacking. It is clearly evident that the first DL follows the FCC stacking and covering about Θ_{FCC} 70% of the surface area. The fit quality achieved for different models such as HCP-type or mixed growth is distinctly worse. From the variance of the GOF, we estimate that the accuracy of the occupancy determination is in the 10–20 percentage point

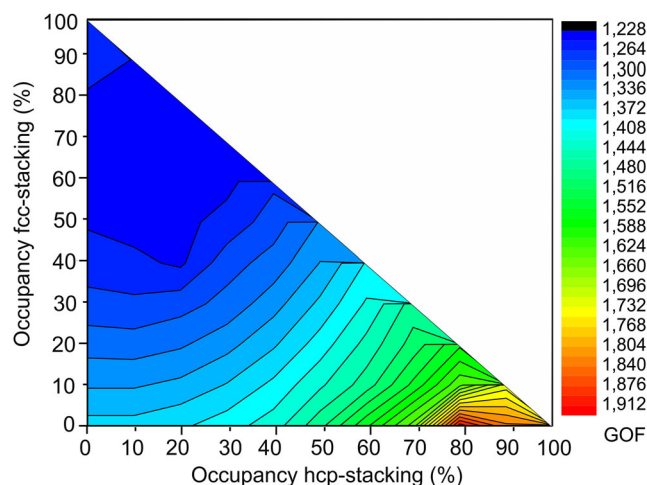


Figure 6. Contour plot of the fit quality versus fractional occupancy of the first DL in FCC and HCP stacking indicating clear evidence for the first DL being stacked in FCC-type relative to the Bi₂Se₃(0001) surface.

regime. The GOF minimum is approximately at $\Theta_{\text{HCP}} = 15\%$ HCP occupancy, which however appears as not being significant.

Furthermore, no atomic exchange between europium and bismuth as well as intercalation of europium into the first van der Waals (vdW) gap is found (at least within the uncertainty estimated). In this respect, the EuS/Bi₂Se₃ interface is distinctly different to many other metallic adsorbates where extensive alloying with bismuth has been found, such as, in the case of iron, gold, silver, and chromium.^[24,25,28,30]

The second DL (fractional occupancy $\approx 45\%$) grows on the first one in a FCC-type stacking, although the HCP-type stacking cannot be ruled out based on the XRD analysis alone, as it yields almost the same GOF and very similar structural z -parameters. This is because of the low occupancy and the very large ADPs (see the following paragraphs). As will be shown later, theory favors the FCC stacking having a lower total energy. The HCP-type stacking of the second DL would not come as a surprise and we recall that stacking faults at the surface of ultrathin films of bulk rocksalt-type insulators growing along the polar [111] direction have been reported in the past. One example is the rocksalt-type CoO on Ir(001).^[43] The stacking fault, there in detail induced by a switch from the bulk-like FCC stacking to the Wurtzite-type stacking was inferred to turn the insulating film to metallic, thereby contributing to the depolarization of the polar structure.^[44]

Vertical relaxations are important within the EuS film and the first QL of the substrate albeit being small. For the latter, a value of $d_{12} = 1.54 \pm 0.12 \text{ \AA}$ is found, which corresponds to a -3% contraction relative to the bulk value of $d = 1.587 \text{ \AA}$.^[23] Spacings between deeper layers are also little affected and only d_{23} , which is equal to 2.10 ± 0.05 versus 1.94 \AA in the bulk, exhibits an expansion outside the experimental uncertainty.

Within the EuS film, we observe strong relaxations. In bulk EuS, the distance between consecutive europium and sulfur layers is equal to 1.722 \AA , whereas we find 1.79 ± 0.16 , 1.66 ± 0.19 , and $2.53 \pm 0.29 \text{ \AA}$ within the film and $2.15 \pm 0.18 \text{ \AA}$ between selenium atom and europium at the interface. The experimental uncertainty for the topmost spacing ($2.35 \pm 0.29 \text{ \AA}$) within the EuS film is quite large due to the small contribution of the sulfur atom to the total scattering amplitude, whereas the others are

more accurate. We, therefore, discuss the latter only. In the interior of the EuS film, the vertical height of the center EuS DL is equal to 3.45 Å, which is almost identical to the corresponding value in the bulk (3.444 Å). A large expansion is not expected due to the fact that the EuS film is only under small compressive strain of $\epsilon_{\parallel} = -1.9\%$ (in-plane lattice parameter 4.22 Å vs 4.14 Å for EuS and Bi₂Se₃, respectively). In parallel with the vertical relaxation, the Eu–S bond distances are modified from the bulk value (2.984 Å) to 2.91 Å and 2.98 Å ($\pm 0\%$ and -2.5% , respectively) within the film, whereas the Eu–Se distance at the interface is equal to 3.21 Å, which is 4% larger than in bulk EuSe (3.096 Å).

Simultaneously with atomic relaxations the Debye parameters (B) were refined. For atoms within the EuS film they are in the range between $B = 10$ and 15 \AA^2 corresponding to isotropic mean-squared displacement amplitudes of $U = 0.13$ and 0.19 \AA^2 , respectively. These very high values can only be related to static disorder rather than to thermal disorder which is typically in the $B = 0.5\text{--}1 \text{ \AA}^2$ range.

We recall that the CTR analysis is sensitive to the structure of the overlayer atoms relative to the (1×1) surface unit cell. This corresponds to a projection of all adlayer atomic sites within the experimental coherence length (several hundred nanometers) into the (1×1) surface unit cell.^[45] STM images in Figure 2 show isolated EuS islands rather than a film completely covering the substrate surface. Based on this observation, we may tentatively suggest that due to the high surface-to-volume ratio of the islands, the large fraction of atoms located near the island rims locally relax laterally. In consequence, these are not in perfect registry with the (1×1) surface unit cell. This scenario is referred to as “mesoscopic misfit” (MM) and has been observed in many nanoislands systems.^[45–47]

4. Ab Initio Calculations

To elucidate the experimental findings, we resort to a density functional theory (DFT) approach to describe electronic and magnetic properties of the EuS/Bi₂Se₃(0001) interface. The approach is a self-consistent relativistic full-potential Green function method based on the multiple-scattering theory and provides an adequate description of bulk materials, surface, interfaces, and real-space clusters.^[48–50] The goal of our simulations is to study 2 DL of EuS on Bi₂Se₃(0001). The structure model, derived by SXRD, serves as input for our calculations, which are carried out within a generalized gradient approximation (GGA) of the DFT.^[51] To eliminate the polarity of the EuS surface, dangling bonds at the S-terminated side of the slab were passivated by hydrogen atoms as suggested Eremeev et al.^[32] The strongly localized Eu 4f electrons are treated within the GGA+ U approach.^[52] The effective Hubbard parameter $U^* = U - J = 5$ eV was chosen to ensure the binding energy of Eu 4f states to be in agreement with available photoemission experiments.^[53,54] To verify the value of U^* , we calculated various magnetic properties of EuS bulk. The obtained magnetic moment $\mu_{\text{Eu}}^{\text{theory}} = 6.93 \mu_{\text{B}}$ and the Curie temperature $T_{\text{C}}^{\text{theory}} = 15.3$ K are in good agreement with experimental results, $\mu_{\text{Eu}}^{\text{exp}} \approx 7 \mu_{\text{B}}$ and $T_{\text{C}}^{\text{exp}} = 16.3$ K, respectively.^[55]

The EuS/Bi₂Se₃(0001) interface was simulated with a symmetric supercell consisting of six Bi₂Se₃ QLs, four EuS DLs

(placed by two on both sides of the Bi₂Se₃ slab), and four vacuum QLs. The vacuum layers were represented by empty ($Z = 0$) Wigner–Seitz cells. The angular momentum cutoff for the Green function expansion was chosen to be $l_{\text{max}} = 3$. For the integration over the Brillouin zone (BZ), we used an improved tetrahedron method with a $20 \times 20 \times 6$ mesh in the full BZ.^[56] As the stacking of the second EuS DL relative to the that of the first one adjacent of the Bi₂Se₃(0001) surface (“FCC” vs “HCP”) could not unambiguously determined by SXRD total energy calculations were carried out, indicating that the FCC stacking is energetically more favorable than the HCP stacking by 0.4 eV per unit cell. At first view, this suggests that the FCC stacking is favored, but we recall that growth of ultrathin adlayers on a substrate crystal is a highly nonequilibrium process, so that a HCP-type stacking cannot be excluded a priori. Therefore, we studied both stacking sequences and compare their impact on the electronic and magnetic properties of the film.

To describe the magnetic properties of the two DL thick EuS/Bi₂Se₃(0001) system the exchange parameters between magnetic moments were calculated using the magnetic force theorem as implemented within the multiple scattering theory.^[57,58] Due to the lack of itinerant electrons, the magnetic interaction is not expected to be of long-range order. Therefore, any magnetic configuration can be used as a reference. As EuS is known to be an FM insulator, we chose this type of ordering for the estimate of the exchange coupling parameters $J(\mathbf{R})$.

The magnetic moment of Eu atoms (μ_{Eu}) is primarily determined by the occupied 4f electrons in the majority spin channel (Figure 7) and is equal to $\mu_{\text{Eu}} = 6.9 \mu_{\text{B}}$. We find a strong magnetic moment for the surface sulfur atom being equal to $\mu_{\text{Se}} = 0.6 \mu_{\text{B}}$ originating from the unpaired S- p_z states at the film surface (see topmost panels in Figure 7). This scenario bears close resemblance with the oxygen- p_z -derived magnetic moment in polar ZnO.^[59,60] Magnetic moments for top-layer sulfur are almost identical for FCC- and HCP-type stacking of the second DL.

The surface sulfur possesses a large density of states (DOS) in the vicinity of the Fermi level (E_{F}) indicating a metallic surface and eliminating the polarity. It should be emphasized that this does not depend on whether the surface sulfur atoms are passivated by hydrogen or not. As Bi₂Se₃ is known to have natural defects such as Se vacancies etc. acting as n-doping, we considered both the undoped (pristine) and the n-doped case. The natural n-doping in Bi₂Se₃ leads to an energetic shift of the DOS by $\approx 0.3\text{--}0.4$ eV toward the conduction band. In our calculations, n-doping is considered by a small concentration of Se vacancies either within the coherent potential approximation^[61,62] or by shifting the DOS toward the conduction bands. Both approaches provide very similar results.

Exchange coupling parameters (J_{ij}) for both FCC- and HCP-stacking models as well as for undoped and n-doped Bi₂Se₃ are shown in Figure 4 versus the interatomic distance (D) between atomic pairs. First of all, the overall behavior of the J_{ij} is that increasing D decreases the J_{ij} rapidly while being oscillatory in nature, typical for the RKKY interaction.^[63] Furthermore, large magnetic exchange parameters are only observed for the second (top) EuS DL, whereas they are almost negligible for the first (interface) DL. Therefore, the magnetic coupling between europium moments is FM in nature

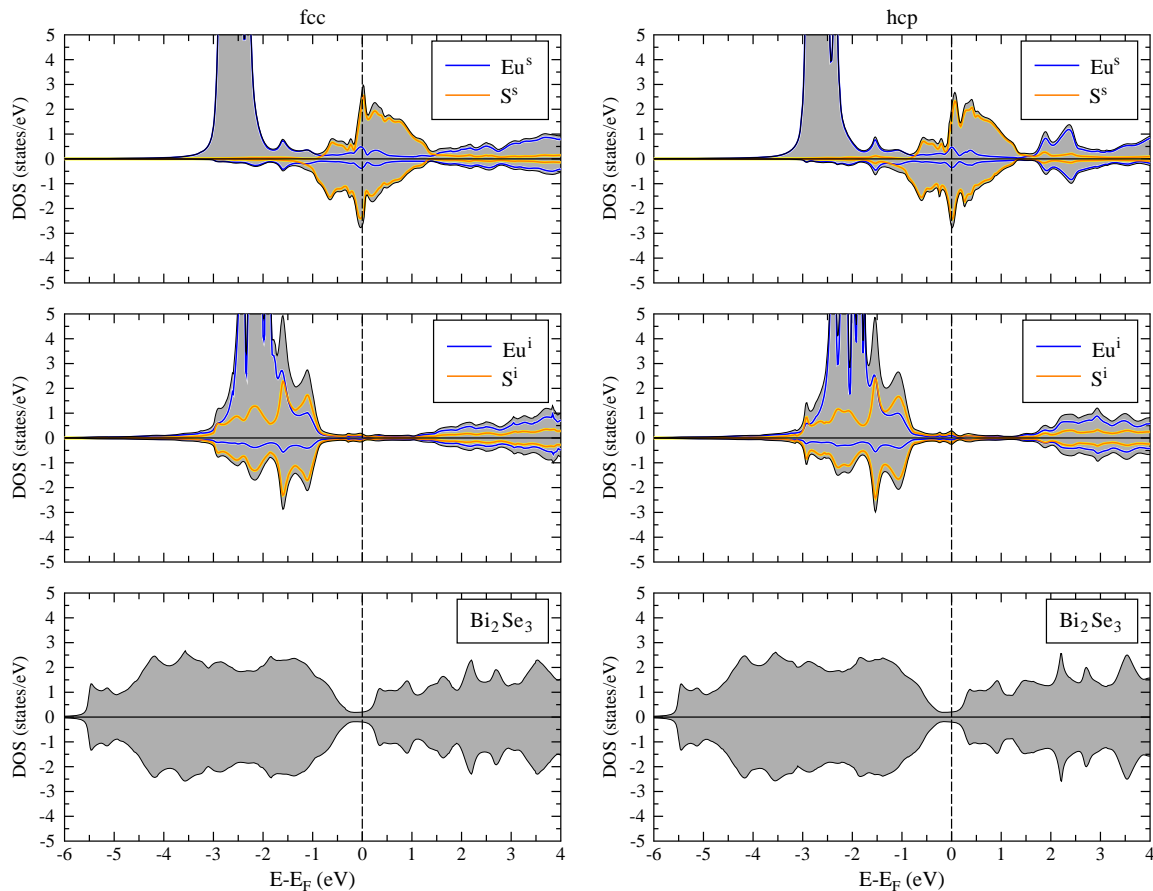


Figure 7. Calculated layer- and spin-resolved DOS of EuS/Bi₂Se₃(0001) for FCC (left panel) and HCP (right panel) stacking of the second EuS DL. Panels from the top to the bottom represent DOS of the surface DL, the interface DL, and the first QL of Bi₂Se₃, respectively. Subscripts s and i means atoms in the surface and interface layers, respectively.

(i.e., $J_{\text{Eu-Eu}} > 0$) but very weak (see black open and filled symbols in **Figure 8**). This is almost independent on the Bi₂Se₃ doping state as the DOS related to the itinerant electrons is almost constant within the corresponding energy range. Furthermore, the magnetic interaction between the localized europium 4f electrons is primarily mediated by itinerant 5d states, which are almost unoccupied in this system. In consequence, $J_{\text{Eu-Eu}}$ is nearly identical in both stacking sequences and for both EuS DLs. Based on the random phase approximation, we estimated the Curie temperature (T_C) of the europium subsystem—while eliminating the exchange coupling with sulfur—and found $T_C = 2 - 3$ K for both stacking sequences and almost independent on doping (the sulfur is excluded from the consideration).

Magnetic coupling between sulfur ($J_{\text{S-S}}$) and between europium and sulfur ($J_{\text{Eu-S}}$) is strongly affected by doping (see open and filled symbols in Figure 4, respectively). The most interesting result of the calculations is the large magnetic moment of sulfur in the surface EuS DL. As pointed out previously, the sulfur magnetic moment is generated by the unpaired S- p_z electrons. Depending on the doping state, the nearest neighbor exchange parameter $J_{\text{S-S}}$ is either negative ($J_{\text{S-S}} = -6.5$ meV) or positive ($J_{\text{S-S}} = +4.0$ meV), for undoped and doped Bi₂Se₃, respectively. It is, however, almost independent on the stacking sequence.

Thus, for the undoped case, the sulfur moments order antiparallel to each other, whereas they are parallel due to the n-doping. For the latter case, T_C was found to be 194 and 198 K for the FCC and HCP stackings, respectively. As Bi₂Se₃ samples are naturally n-doped, the parallel orientation of the moments should be observed in experiment. The sulfur magnetic moments do not significantly differ depending on doping: $\mu = 0.58 \mu_B$ versus $0.60 \mu_B$ in the undoped case. The origin for the strong dependency of the sign of $J_{\text{S-S}}$ on the doping state are variations of the DOS near E_F induced by doping where the sulfur moments are becoming more localized and the interaction between them is getting more short range.

Nearest neighbor exchange parameters between sulfur and europium are positive and strong in the case of undoped Bi₂Se₃: $J_{\text{Eu-S}} = 9.4$ and 7.5 meV for FCC and HCP stacking, respectively. Note that, this is opposite in sign to $J_{\text{S-S}}$. Europium moments in the interfacial EuS layer are weakly coupled to the Eu moments in the surface layer and try to order parallel to each other. As the Eu-Eu interaction is very weak, it is difficult to maintain a certain stable magnetic order for the Eu_i moments. The estimated Néel temperature (T_N) for the FCC- and HCP-stacking model in the absence of doping is $T_N = 210$ and 226 K, respectively.

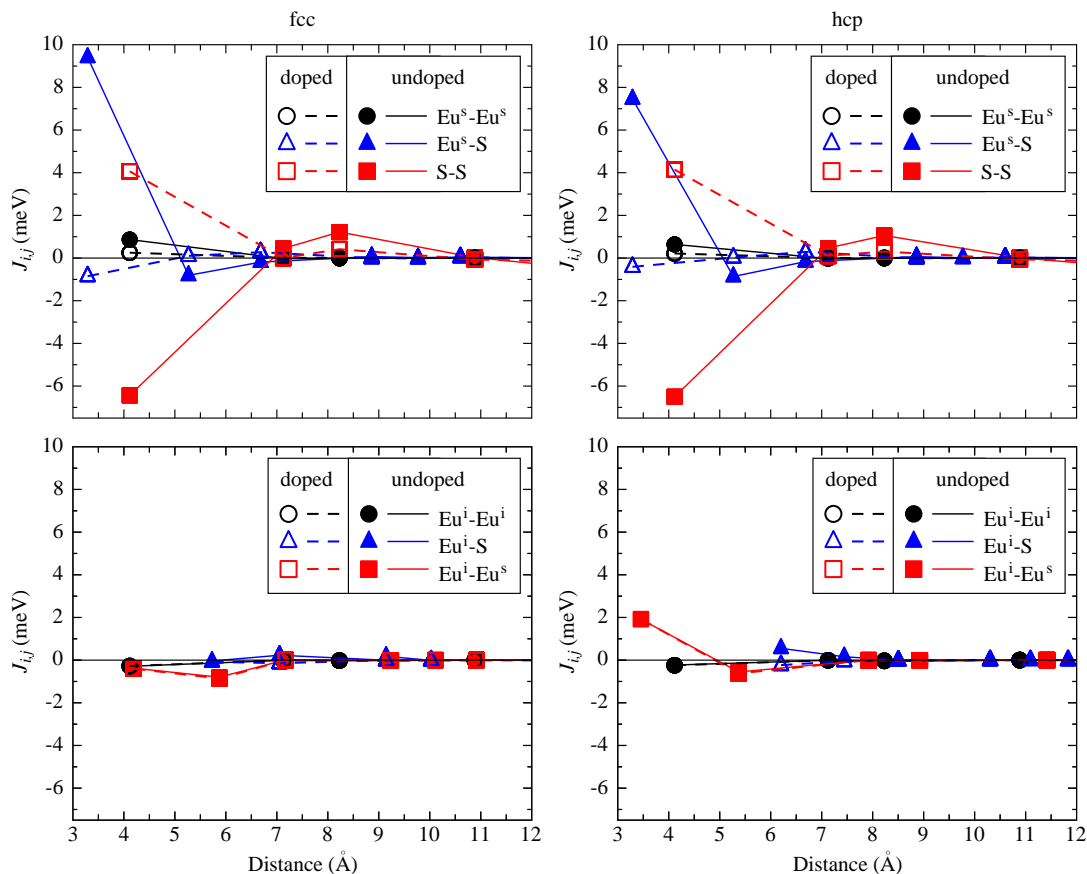


Figure 8. Calculated exchange coupling parameters between europium and surface sulfur in EuS/Bi₂Se₃(0001) with FCC (left panel) and HCP (right panel) stacking of the top EuS DL. Subscripts s and i means atoms in the surface and interface layers, respectively.

5. Conclusions

In summary, we have carried out a combined experimental and theoretical study of a 2 DL thick EuS film and its interface to the Bi₂Se₃(0001) surface. EuS grows in a single domain state with europium of the first EuS DL on the FCC sites on the Bi₂Se₃(0001) surface, i.e., above the third-layer selenium atoms of the first QL. The second DL continues the FCC-type stacking. The electronic structure of the EuS film is characterized by a metallic surface DL lifting polarity, whereas the magnetic interaction is dominated by the RKKY interaction. Most importantly, we find that there is a strong p_z -orbital-derived magnetic moment ($\approx 0.6 \mu_B$) for the top-layer sulfur atoms due to the dangling bonds, which is not quenched upon passivation by hydrogen. Magnetic coupling parameters J_{ij} are weak between europium atoms, but strong (4–9 meV) between sulfur and sulfur and between europium and sulfur magnetic moments. The magnetic interaction between sulfur magnetic moments is strong, extended over several coordination spheres and can establish a certain magnetic order in the system: an antiferromagnetic order in the absence of n-doping and the FM one under n-doping, which is natural for Bi₂Se₃ samples. Critical temperatures were estimated within the range of 194–226 K depending on the doping and on the type of stacking (either FCC or HCP)

sequences. In real experiments, the value of the critical temperature can be higher due to presence of various defects, which could be responsible for a certain magnetic order as it was already found in other systems.^[59,60,64–67]

Acknowledgements

This work was supported by the Deutsche Forschungsgemeinschaft (DFG) through priority program SPP 1666. The authors thank M.B. Babanly and K.A. Kokh for supplying the bulk single crystal samples. Technical support by Frank Weiß is gratefully acknowledged. H.L.M. and K.M. thank the staff of Soleil Synchrotron for their hospitality and support during their visit in St. Aubin (France). Open access funding enabled and organized by Projekt DEAL.

Conflict of Interest

The authors declare no conflict of interest.

Keywords

europium sulfide, proximity, surface X-ray diffraction, topological insulators

Received: May 29, 2020

Revised: July 6, 2020

Published online: August 13, 2020

- [1] C. Z. Chang, J. Zhang, X. Feng, J. Shen, Z. Zhang, M. Guo, K. Li, Y. Ou, P. Wei, L. L. Wang, Z. Q. Ji, Y. Feng, S. Ji, X. Chen, J. Jia, X. Dai, Z. Fang, S. C. Zhang, K. He, Y. Wang, L. Lu, X. C. Ma, Q. K. Xue, *Science* **2013**, *340*, 167.
- [2] C. Z. Chang, W. Zhao, D. Y. Kim, H. Zhang, B. A. Assaf, D. Heiman, S. C. Zhang, C. Liu, M. H. W. Chan, J. S. Moodera, *Nat. Mater.* **2015**, *14*, 473.
- [3] J. Wang, B. Lian, S. C. Zhang, *Phys. Scr.* **2015**, *T164*, 014003.
- [4] S. Grauer, S. Schreyeck, M. Winnerlein, K. Brunner, C. Gould, L. W. Molenkamp, *Phys. Rev. B* **2015**, *92*, 201304.
- [5] S. Qi, Z. Qiao, X. Deng, E. D. Cubuk, H. Chen, W. Zhu, E. Kaxiras, S. B. Zhang, X. Xu, Z. Zhang, *Phys. Rev. Lett.* **2016**, *117*, 056804.
- [6] P. P. J. Haazen, J. B. Laloe, T. J. Nummy, H. J. M. Swagten, P. Jarillo-Herrero, D. Heiman, J. S. Moodera, *Appl. Phys. Lett.* **2012**, *100*, 082404.
- [7] F. Yang, Y. R. Song, H. Li, K. F. Zhang, X. Yao, C. Liu, D. Qian, C. L. Gao, J. F. Jia, *Phys. Rev. Lett.* **2013**, *111*, 176802.
- [8] M. G. Vergniory, M. M. Otrokov, D. Thonig, M. Hoffmann, I. V. Maznichenko, M. Geilhufe, X. Zubizarreta, S. Ostanin, A. Marmodoro, J. Henk, W. Hergert, I. Mertig, E. V. Chulkov, A. Ernst, *Phys. Rev. B* **2014**, *89*, 165202.
- [9] Z. Liu, X. Wei, J. Wang, H. Pan, F. Ji, F. Xi, J. Zhang, T. Hu, S. Zhang, Z. Jiang, W. Wen, Y. Huang, M. Ye, Z. Yang, S. Qiao, *Phys. Rev. B* **2014**, *90*, 094107.
- [10] W. Liu, D. West, L. He, Y. Xu, J. Liu, K. Wang, Y. Wang, G. van der Laan, R. Zhang, S. Zhang, K. L. Wang, *ACS Nano* **2015**, *9*, 10237.
- [11] C. Z. Chang, P. Tang, Y. L. Wang, X. Feng, K. Li, Z. Zhang, Y. Wang, L. L. Wang, X. Chen, C. Liu, W. Duan, K. He, X. C. Ma, Q. K. Xue, *Phys. Rev. Lett.* **2014**, *112*, 056801.
- [12] A. I. Figueroa, G. van der Laan, L. J. Collins-McIntyre, G. Cibin, A. J. Dent, T. Hesjedal, *J. Phys. Chem. C* **2015**, *119*, 17344.
- [13] A. I. Figueroa, G. van der Laan, L. J. Collins-McIntyre, S. L. Zhang, A. A. Baker, S. E. Harrison, P. Schönherr, G. Cibin, T. Hesjedal, *Phys. Rev. B* **2014**, *90*, 134402.
- [14] A. A. Baker, A. I. Figueroa, K. Kummer, L. J. Collins-McIntyre, T. Hesjedal, G. van der Laan, *Phys. Rev. B* **2015**, *92*, 094420.
- [15] Z. Liu, X. Wei, J. Wang, H. Pan, F. Ji, M. Ye, Z. Yang, S. Qiao, *Phys. Rev. B* **2015**, *92*, 100101.
- [16] M. Ye, W. Li, S. Zhu, Y. Takeda, Y. Saitoh, Y. Wang, H. Pan, M. Nurmamat, K. Sumida, F. Ji, Z. Liu, H. Yang, Z. Liu, D. Shen, A. Kimura, S. Qiao, X. Xie, *Nat. Commun.* **2015**, *6*, 1.
- [17] L. J. Collins-McIntyre, S. E. Harrison, P. Schönherr, N. J. Steinke, C. J. Kinane, T. R. Charlton, D. Alba-Veneroa, A. Pushp, A. J. Kellock, S. S. P. Parkin, J. S. Harris, S. Langridge, G. van der Laan, T. Hesjedal, *EPL* **2014**, *107*, 57009.
- [18] E. O. Lachman, A. F. Young, A. Richardella, J. Cuppens, H. R. Naren, Y. Anahory, A. Y. Meltzer, A. Kandala, S. Kempinger, Y. Myasoedov, M. E. Huber, N. Samarth, E. Zeldov, *Sci. Adv.* **2015**, *1*, e1500740.
- [19] L. Zhang, D. Zhao, Y. Zang, Y. Yuan, G. Jiang, M. Liao, D. Zhang, K. He, X. Ma, Q. Xue, *APL Mater.* **2017**, *5*, 076106.
- [20] J. Henk, M. Fliieger, I. V. Maznichenko, I. Mertig, A. Ernst, S. V. Eremeev, E. V. Chulkov, *Phys. Rev. Lett.* **2012**, *109*, 076801.
- [21] J. Henk, M. Fliieger, I. V. Maznichenko, I. Mertig, A. Ernst, S. V. Eremeev, E. V. Chulkov, *Phys. Rev. Lett.* **2012**, *109*, 076801.
- [22] S. Roy, H. L. Meyerheim, A. Ernst, K. Mohseni, C. Tusche, M. G. Vergniory, T. V. Menshchikova, M. M. Otrokov, A. G. Ryabishchenkova, Z. S. Aliev, M. B. Babanly, K. A. Kokh, O. E. Tereshchenko, E. V. Chulkov, J. Schneider, J. Kirschner, *Phys. Rev. Lett.* **2014**, *113*, 116802.
- [23] S. Roy, H. L. Meyerheim, K. Mohseni, A. Ernst, M. M. Otrokov, M. G. Vergniory, G. Mussler, J. Kampmeier, D. Grützmacher, C. Tusche, J. Schneider, E. V. Chulkov, J. Kirschner, *Phys. Rev. B* **2014**, *90*, 155456.
- [24] A. Polyakov, H. L. Meyerheim, E. D. Crozier, R. A. Gordon, K. Mohseni, S. Roy, A. Ernst, M. G. Vergniory, X. Zubizarreta, M. M. Otrokov, E. V. Chulkov, J. Kirschner, *Phys. Rev. B* **2015**, *92*, 045423.
- [25] A. Polyakov, H. L. Meyerheim, E. D. Crozier, R. A. Gordon, K. Mohseni, S. Roy, A. Ernst, M. G. Vergniory, X. Zubizarreta, M. M. Otrokov, E. V. Chulkov, J. Kirschner, *Phys. Rev. B* **2015**, *92*, 045423.
- [26] R. Shokri, H. L. Meyerheim, S. Roy, K. Mohseni, A. Ernst, M. M. Otrokov, E. V. Chulkov, J. Kirschner, *Phys. Rev. B* **2015**, *91*, 205430.
- [27] I. Vobornik, U. Manju, J. Fujii, F. Borgatti, P. Torelli, D. Krizmancic, Y. S. Hor, R. J. Cava, G. Panaccione, *Nano Lett.* **2011**, *11*, 4079.
- [28] A. Polyakov, C. Tusche, M. Ellguth, E. D. Crozier, K. Mohseni, M. M. Otrokov, X. Zubizarreta, M. G. Vergniory, M. Geilhufe, E. V. Chulkov, A. Ernst, H. L. Meyerheim, S. S. P. Parkin, *Phys. Rev. B* **2017**, *95*, 180202.
- [29] M. M. Otrokov, A. Ernst, K. Mohseni, H. Fulara, S. Roy, G. R. Castro, J. Rubio-Zuazo, A. G. Ryabishchenkova, K. A. Kokh, O. E. Tereshchenko, Z. S. Aliev, M. B. Babanly, E. V. Chulkov, H. L. Meyerheim, S. S. P. Parkin, *Phys. Rev. B* **2017**, *95*, 205429.
- [30] S. Roy, A. Polyakov, K. Mohseni, H. L. Meyerheim, *Phys. Status Solidi RRL* **2018**, *12*, 1800138.
- [31] P. Wei, F. Katmis, B. A. Assaf, H. Steinberg, P. Jarillo-Herrero, D. Heiman, J. S. Moodera, *Phys. Rev. Lett.* **2013**, *110*, 186807.
- [32] S. Eremeev, V. Menshov, V. Tugushev, E. Chulkov, *J. Magn. Magn. Mater.* **2015**, *383*, 30, Selected papers from the sixth Moscow International Symposium on Magnetism (MISM-2014).
- [33] F. Katmis, V. Lauter, F. S. Nogueira, B. A. Assaf, M. E. Jamer, P. Wei, B. Satpati, J. W. Freeland, I. Eremin, D. Heiman, P. Jarillo-Herrero, J. S. Moodera, *Nature* **2016**, *544*, 513.
- [34] J. Kim, K. W. Kim, H. Wang, J. Sinova, R. Wu, *Phys. Rev. Lett.* **2017**, *119*, 027201.
- [35] J. Riviere, F. Netzer, G. Rosina, G. Strasser, J. Matthew, *J. Electron Spectros. Relat. Phenomena* **1985**, *36*, 331.
- [36] K. Mohseni, H. L. Meyerheim, *Phys. Status Solidi B* **2020**, *257*, 1900605.
- [37] M. v. Laue, *Ann. Phys.* **1936**, *26*, 55.
- [38] I. Robinson, *Phys. Rev. B* **1986**, *33*, 3830.
- [39] J. Drnec, T. Zhou, S. Pintea, W. Onderwaater, E. Vlieg, G. Renaud, R. Felici, *J. Appl. Crystallogr.* **2014**, *47*, 365.
- [40] I. K. Robinson, D. J. Tweet, *Rep. Prog. Phys.* **1992**, *55*, 599.
- [41] U. H. Zucker, E. Perenthaler, W. F. Kuhs, R. Bachmann, H. Schulz, *J. Appl. Crystallogr.* **1983**, *16*, 358.
- [42] W. F. Kuhs, *Acta Cryst. A* **1992**, *48*, 80.
- [43] W. Meyer, D. Hock, K. Biedermann, M. Gubo, S. Müller, L. Hammer, K. Heinz, *Phys. Rev. Lett.* **2008**, *101*, 016103.
- [44] P. W. Tasker, *J. Phys. C* **1979**, *12*, 4977.
- [45] O. Mironets, H. L. Meyerheim, C. Tusche, V. S. Stepanyuk, E. Soyka, P. Zschack, H. Hong, N. Jeutter, R. Felici, J. Kirschner, *Phys. Rev. Lett.* **2008**, *100*, 096103.
- [46] W. Feng, H. L. Meyerheim, K. Mohseni, O. Brovko, V. S. Stepanyuk, N. Jedrecy, R. Felici, J. Kirschner, *Phys. Rev. Lett.* **2013**, *110*, 235503.
- [47] O. O. Brovko, D. I. Bazhanov, H. L. Meyerheim, D. Sander, V. S. Stepanyuk, J. Kirschner, *Surf. Sci. Rep.* **2014**, *69*, 159.
- [48] M. Lüders, A. Ernst, W. M. Temmerman, Z. Szotek, P. J. Durham, *J. Phys.: Condens. Matter* **2001**, *13*, 8587.
- [49] M. Geilhufe, S. Achilles, M. A. Köbis, M. Arnold, I. Mertig, W. Hergert, A. Ernst, *J. Phys.: Condens. Matter* **2015**, *27*, 435202.

- [50] M. Hoffmann, A. Ernst, W. Hergert, V. N. Antonov, W. A. Adeagbo, R. M. Geilhufe, H. Ben Hamed, *Phys. Status Solidi B* **2020**, 1900671.
- [51] J. P. Perdew, K. Burke, M. Ernzerhof, *Phys. Rev. Lett.* **1996**, 77, 3865.
- [52] V. I. Anisimov, J. Zaanen, O. K. Andersen, *Phys. Rev. B* **1991**, 44, 943.
- [53] R. Vercaemst, D. Poelman, L. Fiermans, R. V. Meirhaeghe, W. Lafire, F. Cardon, *J. Electron Spectros. Relat. Phenomena* **1995**, 74, 45.
- [54] Y. Liu, A. Luchini, S. Mart-Snchez, C. Koch, S. Schuwalow, S. A. Khan, T. Stankevi, S. Francoua, J. R. L. Mardegan, J. A. Krieger, V. N. Strocov, J. Stahn, C. A. F. Vaz, M. Ramakrishnan, U. Staub, K. Lefmann, G. Aeppli, J. Arbiol, P. Krogstrup, *Coherent Epitaxial Semiconductor-Ferromagnetic Insulator InAs/EuS Interfaces: Band Alignment and Magnetic Structure*, **2019**.
- [55] P. Schwob, O. Vogt, *Phys. Lett. A* **1967**, 24, 242.
- [56] P. E. Blöchl, O. Jepsen, O. K. Andersen, *Phys. Rev. B* **1994**, 49, 16223.
- [57] A. I. Liechtenstein, M. I. Katsnelson, V. A. Gubanov, *J. Phys. F: Met. Phys.* **1984**, 14, L125.
- [58] A. I. Liechtenstein, M. I. Katsnelson, V. P. Antropov, V. A. Gubanov, *J. Magn. Magn. Mater.* **1987**, 67, 65.
- [59] H. L. Meyerheim, A. Ernst, K. Mohseni, C. Tusche, W. A. Adeagbo, I. V. Maznichenko, W. Hergert, G. R. Castro, J. Rubio-Zuazo, A. Morgante, N. Jedrecy, I. Mertig, J. Kirschner, *Phys. Rev. B* **2014**, 90, 085423.
- [60] G. Fischer, N. Sanchez, W. Adeagbo, Z. Szotek, W. M. Temmerman, A. Ernst, M. Hoffmann, W. Hergert, M. C. Muñoz, *J. Phys.: Condens. Matter* **2015**, 28, 016003.
- [61] P. Soven, *Phys. Rev.* **1967**, 156, 809.
- [62] B. L. Gyorffy, *Phys. Rev. B* **1972**, 5, 2382.
- [63] M. A. Ruderman, C. Kittel, *Phys. Rev.* **1954**, 96, 99.
- [64] M. Khalid, M. Ziese, A. Setzer, P. Esquinazi, M. Lorenz, H. Hochmuth, M. Grundmann, D. Spemann, T. Butz, G. Brauer, W. Anwand, G. Fischer, W. A. Adeagbo, W. Hergert, A. Ernst, *Phys. Rev. B* **2009**, 80, 035331.
- [65] W. A. Adeagbo, G. Fischer, A. Ernst, W. Hergert, *J. Phys.: Condens. Matter* **2010**, 22, 436002.
- [66] G. Fischer, N. Sanchez, W. Adeagbo, M. Lüders, Z. Szotek, W. M. Temmerman, A. Ernst, W. Hergert, M. C. Muñoz, *Phys. Rev. B* **2011**, 84, 205306.
- [67] I. Lorite, B. Straube, H. Ohldag, P. Kumar, M. Villafuerte, P. Esquinazi, C. E. Rodriguez Torres, S. Perez de Heluani, V. N. Antonov, L. V. Bekenov, A. Ernst, M. Hoffmann, S. K. Nayak, W. A. Adeagbo, G. Fischer, W. Hergert, *Appl. Phys. Lett.* **2015**, 106, 082406.